Journal of Alloys and Compounds 525 (2012) 87–96

Contents lists available at SciVerse ScienceDirect

Journal of Alloys and Compounds

journal homepage: www.elsevier.com/locate/jallcom

Thermal cycling behavior of YSZ and $La_2(Zr_{0.7}Ce_{0.3})_2O_7$ as double-ceramic-layer systems EB-PVD TBCs

Zhenhua Xu[a,*], Limin He[a], Rende Mu[a], Feng Lu[a], Shimei He[a], Xueqiang Cao[b]

[a] Beijing Institute of Aeronautical Materials, Department 5, P.O. Box 81-5, Beijing 100095, China
[b] State Key Laboratory of Rare Earth Resource Utilization, Changchun Institute of Applied Chemistry, Chinese Academy of Sciences, Changchun 130022, China

ARTICLE INFO

Article history:
Received 20 January 2012
Received in revised form 6 February 2012
Accepted 12 February 2012
Available online xxx

Keywords:
Thermal barrier coatings
Double-ceramic-layer
EB-PVD
$La_2(Zr_{0.7}Ce_{0.3})_2O_7$
Thermal cycling

ABSTRACT

Double-ceramic-layer (DCL) thermal barrier coatings (TBCs) of $La_2(Zr_{0.7}Ce_{0.3})_2O_7$ (LZ7C3) and yttria stabilized zirconia (YSZ) were deposited by electron beam-physical vapor deposition (EB-PVD). The thermal cycling test at 1573 K in burner-rig with a coal gas flame indicates the thermal cycling life of DCL coating is not only much longer than that of LZ7C3 coating, but also approximately 27% longer than that of YSZ coating. The superior sintering-resistance of LZ7C3 coating and the unique growth modes of columns within DCL coating are all very helpful to the prolongation of thermal cycling life of DCL coating. The failure of DCL coating is mainly a result of the reduction–oxidation of cerium oxide, the re-crystallization of some LZ7C3 fine grains, the cracks initiation, propagation and extension, the abnormal oxidation of bond coat, the degradation of t'-phase in YSZ coating and the outward diffusion of Cr alloying element into LZ7C3 coating. Since no single material that has been studied so far satisfies all the requirements for high temperature applications, DCL coating is an important development direction of TBCs.

1. Introduction

Ceramic coatings are widely served as thermal, wear and corrosion barriers in modern industries. Wherein, thermal barrier coatings (TBCs) are playing an important role in the development of the next generation aerospace gas-turbine engines. TBCs provide thermal protection to superalloy blades and enable engines to be operated at higher gas inlet temperature, giving rise to the improvements of the thrust-to-weight ratio, lifetime and fuel efficiency of the aerospace engines. Currently, a TBC system consists of two layers, including a superalloy bond coat (MCrAlY, M = Ni, Co) as the oxidation resistant layer and a ceramic top-coat as the heat resistant layer. The mismatch of thermal and mechanical properties between the bond coat and ceramic coating is the key factor to determine the performance of TBCs. The moderate coefficient of thermal expansion (CTE) compared to that of bond coat ($\sim 14 \times 10^{-6}\,K^{-1}$) [1] and low thermal conductivity are the first two selection criteria of TBC candidate materials. Nowadays, plasma spraying (PS) and electron-beam physical vapor deposition (EB-PVD) are the two main methods for the fabrication of TBCs.

6–8 wt% yttria stabilized zirconia (YSZ) is the state-of-the-art ceramic top-coat TBC material. However, as the temperature within gas turbine engines increases, the continued use of YSZ has become problematic. The primary concerns arise from [2]: (i) accelerated sintering kinetics of porous YSZ (which decreases the pore content of the TBCs and thus its in-plane compliance and thermal resistance); (ii) de-stabilization of the desirable non-transformable t' phase that is responsible for the intrinsic toughness of YSZ; and (iii) an increased propensity for penetration of the coating by molten deposits of calcium–magnesium-alumino-silicates (CMAS) which dissolve the coating and accelerate YSZ destabilization. Upon solidification, these deposits degrade the strain tolerance of the coating and lead to premature failure. These concerns, coupled with the potential design benefits of further reductions of the thermal conductivity relative to YSZ, have motivated a far-reaching search for alternate thermal barrier oxides. As a result, some other metal oxides such as CeO_2, Sc_2O_3, In_2O_3, Ta_2O_5 and Re_2O_3 (Re = La, Nd, Sm, Gd, Dy and Yb) doped ZrO_2 counterparts have been developed for various purposes of enhancing the phase stability or the corrosion resistances [3,4].

On the other hand, new TBC candidate materials such as the pyrochlore-type rare earth zirconates ($Re_2Zr_2O_7$, Re = La, Nd, Sm and Gd) with low thermal conductivity, high phase stability and moderate coefficient of thermal expansion (CTE), the fluorite-type $Re_2Ce_2O_7$ (Re = La and Nd) have also been proposed and extensively studied for potential applications [1–7]. Especially those materials with the mixture of pyrochlore and fluorite structures, lanthanum–zirconium–cerium composite oxide ($La_2(Zr_{0.7}Ce_{0.3})_2O_7$, LZ7C3) shows promising thermo-physical properties and has attracted a great attention. Bulk LZ7C3 has a

* Corresponding author. Tel.: +86 10 62496456; fax: +86 10 62496456.
E-mail address: zhxuciac@yahoo.com (Z. Xu).

0925-8388/$ – see front matter © 2012 Elsevier B.V. All rights reserved.
doi:10.1016/j.jallcom.2012.02.079

lower thermal conductivity (0.87 W m^{-1} K^{-1}, 1273 K) than that of YSZ (2.1–2.2 W m^{-1} K^{-1}, 1273 K) as reported by Sodeoka [8]. It is thermally stable up to its melting point (~2413 K), and it has been proposed as a promising TBCs material [9,10]. However, the relatively low thermal expansion coefficient of LZ7C3 from room temperature to 1673 K leads to high thermal stress between the LZ7C3 coating and the metallic bond coat, and the chemical compatibility of LZ7C3 coating and thermally grown oxide (TGO) layer is unstable during thermal cycling test. Therefore, the single LZ7C3 coating usually has a short thermal cycling life as reported in previous papers [10,11]. In addition, the rare earth zirconates suffer two fundamental disadvantages relative to YSZ. Firstly, $Re_2Zr_2O_7$ is susceptible to reaction with the alumina TGO [2,12], resulting in the formation of aluminate interphases by diffusional reactions. Secondly, as with the cubic ZrO_2-based phases, the rare earth zirconates exhibit a substantially lower toughness than the tetragonal t' phase of YSZ [2,13]. This has deleterious consequences for both their erosion resistance and other failure mechanisms that involve crack propagation through the TBCs.

To alleviate the aluminate reaction problem, the double-ceramic-layer (DCL) coating of $La_2Zr_2O_7$ (LZ) and YSZ (LZ/YSZ, the LZ layer is formed on top of the YSZ layer) has been proposed and prepared via PS by Vassen [14] and Cao [15]. In the DCL coating, the top ceramic layer should have a low thermal conductivity and high phase stability, and it acts as a thermal insulator to protect the inner layer. However, little is known about the factors governing the delamination resistance of those DCL coatings upon thermal cycling at temperatures of relevance in gas turbine engines. In our former work, the failure of DCL LZ7C3/YSZ coating and its thermal cycling lifetime tested at 1373 K in an air furnace were studied [16]. To meet the requirements of the next generation of advanced engines, as a continuing work, the optimized EB-PVD processing conditions were adopted for deposition of the DCL coating of LZ7C3/YSZ and its thermal cycling behavior was tested at 1573 K in burner-rig with a coal gas flame, and then the failure mechanism was also studied.

2. Experimental

2.1. Ingot of LZ7C3 coating

Ingot powder with the desired composition was synthesized by solid-state reaction at 1673 K for 12 h with La_2O_3 (99.99%, Shenghua Chemicals of Hunan), CeO_2 (99.99%, Shenghua Chemicals of Hunan) and ZrO_2 (99.9%, Dongfang Chemicals of Guangdong) as the starting materials. A deionized water-based suspension of ingot powder was ball-milled for 24 h with zirconia balls. The suspension was completely dried in a model with a diameter of 80 mm. After the cast-formation, the ingot was densified at 1773 K for 12 h. The commercial ingot of YSZ (GRINM, Beijing) was directly used for the deposition of YSZ layer.

2.2. Preparation of bond coat and top ceramic coating

The directionally-solidified Ni-based superalloy DZ125 (diameter = 30 mm, thickness = 3 mm) was used as the substrate material. The substrates were ground before the bond coat (BC) of NiCrAlYSi was deposited by arc ion-plating (A-1000 Vacuum Arc Ion-Plating Unit). The BC used identically in this study had a nominal composition (wt%): 20–25Cr, 6–10Al, 0.08–0.4Y, 0.4–0.8Si, and Ni as balance. After the deposition of BC, the substrates were heat-treated under high vacuum at 1143 K for 3 h. The purpose of heat treatment at 1143 K before EB-PVD deposition was to enhance the adhesion of bond coat to substrate due to interdiffusion between them. The YSZ coating was firstly deposited onto BC followed by the deposition of LZ7C3 coating. The current of electron beam used in this study was in range of 500–700 mA. Meanwhile, the accelerated high-voltage (kV) was in the range of −9.52 to −10.91. The average thicknesses of YSZ and LZ7C3 coatings were about 250 μm and 200 μm, respectively. The deposition pressure of EB-PVD working chamber was about 5×10^{-3} Pa and no oxygen was introduced into the vacuum chamber. The average substrate temperature was 1223 ± 25 K and the rotation speed was 20 rpm.

2.3. Thermal cycling tests

Thermal cycling tests of the coating samples were performed using burner-rig equipment with a coal gas flame. The thermal cycling test of the coating was finished by heating the coating surface from room temperature to 1573 ± 30 K for 5 min followed by quenching for 2 min by a compressed air jet, while the substrate temperatures was at 1253 ± 15 K during heating. This process was repeated until a clearly visible coating surface area of 5% was lost, and the cyclic number was then regarded as the thermal cycling lifetime of TBCs. Infrared-radiation pyrometer (λ = 9.6–11.5 μm) was used to monitor the surface temperature of the coating, and the substrate temperature was measured by a standard Pt/Pt–Rh_{10} thermal couple.

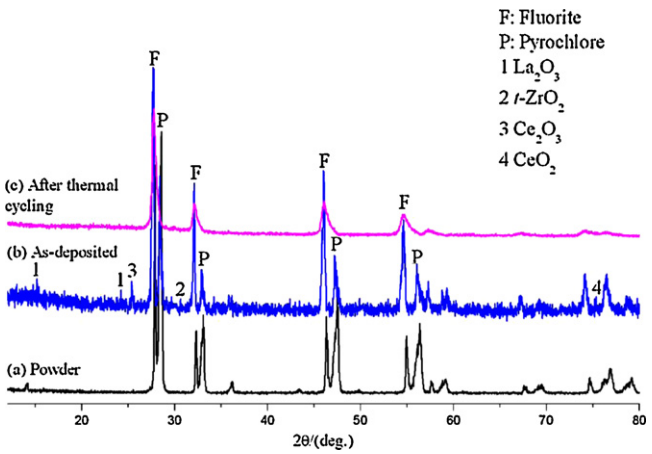

Fig. 1. XRD patterns of LZ7C3 powder (a), and DCL coating surface before (b) and after (c) thermal cycling.

2.4. Characterizations

The coating samples were embedded in a transparent cold-setting epoxy and then sectioned, ground and polished with diamond pastes down to 1 μm. Scanning electron microscope (SEM, FEI-Quanta 600) equipped with EDS (Oxford INCAx-sight 6427) was applied for the microstructure and composition evaluation.

X-ray diffraction (XRD, Bruker D8 Advance) with Cu Kα radiation at a scan rate of 4° min^{-1} was used for the phase determination of powders and coatings. Coatings without polishing were used directly for XRD measurements.

Raman spectrum was recorded at room temperature with T64000 modular triple Raman system (Horiba Jobin Yvon, France). The 514.5 nm line of an argon ion laser (Stabilite 2017, Spectra-Physics Lasers Inc., USA) was used as the excitation line. Laser power of 5 mW was incident on the sample in a 2 μm diameter spot through a standard microscope objective lens. The Raman spectrum was collected with a data point acquisition time of 90 s and a spectral range of 100–1000 cm^{-1}.

3. Results and discussion

3.1. Phase determination

The XRD patterns of the DCL coating surface before and after thermal cycling are compared in Fig. 1. For comparison, XRD pattern of the original powder of LZ7C3 is also presented in Fig. 1. Except for a few weak peaks as marked in Fig. 1b, the as-deposited DCL coating exhibits XRD pattern similar to its original powder. However, intensities of its diffraction peaks are low, indicating that the crystallization is not perfect owing to the fast cooling rate of the electron beam. It can be seen from Fig. 1b that the as-deposited coating is mainly crystallized in cubic pyrochlore and fluorite structures even though several weak peaks of La_2O_3, t'-ZrO_2, Ce_2O_3 and CeO_2 phases are observed. The appearance of these phases is probably attributed to the partial decomposition of LZ7C3 ingot during the overheating of EB-PVD. Partial decomposition of rare earth–zirconia composite oxide could occur during EB-PVD due to different vapor pressures of its compositional oxides, which inevitably leads to composition derivation of the deposited ceramic coating from the original ingot [10,17–19]. In addition, one weak peak of Ce_2O_3 as shown in Fig. 1c completely disappears due to its meta-stable oxidation state. On the other hand, for the as-deposited coating, diffraction peaks which belong to the fluorite structure are stronger than those of pyrochlore structure as shown in Fig. 1b. However, it is reverse in the case of LZ7C3 powder (Fig. 1a). It indicates that a solid solution of LZC ($La_2(Zr_xCe_{1-x})_2O_7$) with

fluorite structure is preferentially formed in DCL coating compared with that of $La_2Zr_2O_7$ with pyrochlore structure. Surprisingly, those peak intensities which belong to the pyrochlore structure observed in Fig. 1b are basically approach to disappear as shown in Fig. 1c, implying that the as-decomposed La_2O_3, ZrO_2 and excess CeO_2 (or formation from the further oxidation of Ce_2O_3) could be incorporated into the coating. As a result, the main fluorite structure of $La_2(Zr_xCe_{1-x})_2O_7$ can be strongly further formed, because the temperature of thermal cycling test adopted in this study is ~1573 K, which is higher than that of temperature investigated in our previous work [16]. This result is in good agreement with the previous investigation by Cao [6]. Simultaneously, it is also interesting to see that all the peaks (Fig. 1b) slightly shift to the lower 2θ-value (the larger d-values) in contrast to that of the powder (Fig. 1a). The main reason is that the former has a higher content of La_2O_3 than the latter. La^{3+} (0.106 nm) has a larger ionic radius than Zr^{4+} (0.072 nm) (or Ce^{4+} (0.092 nm)). Differently, all the peaks scrutinized in Fig. 1c slightly shift to the larger 2θ-value compared with the as-deposited coating, implying that the solubility of ZrO_2 in LZ7C3 coating occurs after long-term exposure.

Laser Raman spectroscopy is a powerful tool to investigate chemical composition in ceramic materials [20]. Fig. 2 shows Raman spectrum of DCL coating surface after thermal cycling in the range of 100–1000 cm^{-1} at room temperature. For this specimen, one Raman band at 455 cm^{-1} is visible, which is very similar to the characteristics of the fluorite $La_2(Zr_xCe_{1-x})_2O_7$ according to the Raman spectrum of pure $La_2Ce_2O_7$. This result is in good agreement with the XRD result shown in Fig. 1c. Meanwhile, one Raman band at 254 cm^{-1} is also detected in this specimen. This Raman band is the characteristics of t'-YSZ structure, which is consistent with the previous results [21]. The appearance of t'-YSZ in Fig. 2 may be related to the spallation zone of DCL coating which occurs at the interface of LZ7C3 and YSZ. On the other hand, one Raman band at 551 cm^{-1} is assigned to CeO_2 as shown in Fig. 2. It demonstrates that the solid solution of ZrO_2 (or La_2O_3) into CeO_2 lattice perhaps occurs after long-term exposure. Hence it is reasonable to explain why Raman peak belonging to the fluorite-type structure is very strong.

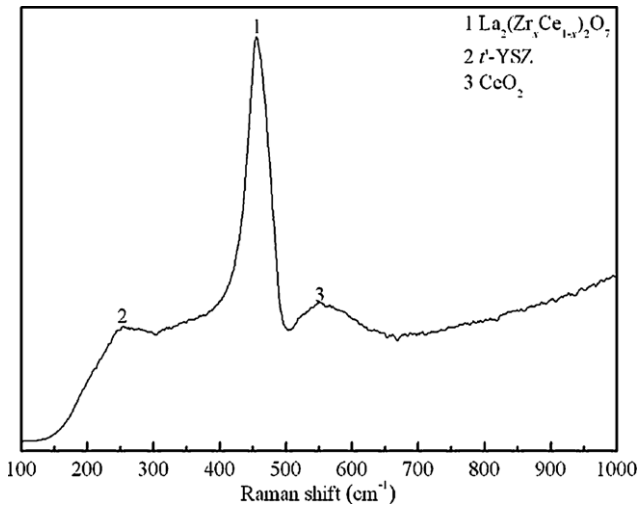

Fig. 2. Raman spectrum of DCL coating surface after thermal cycling.

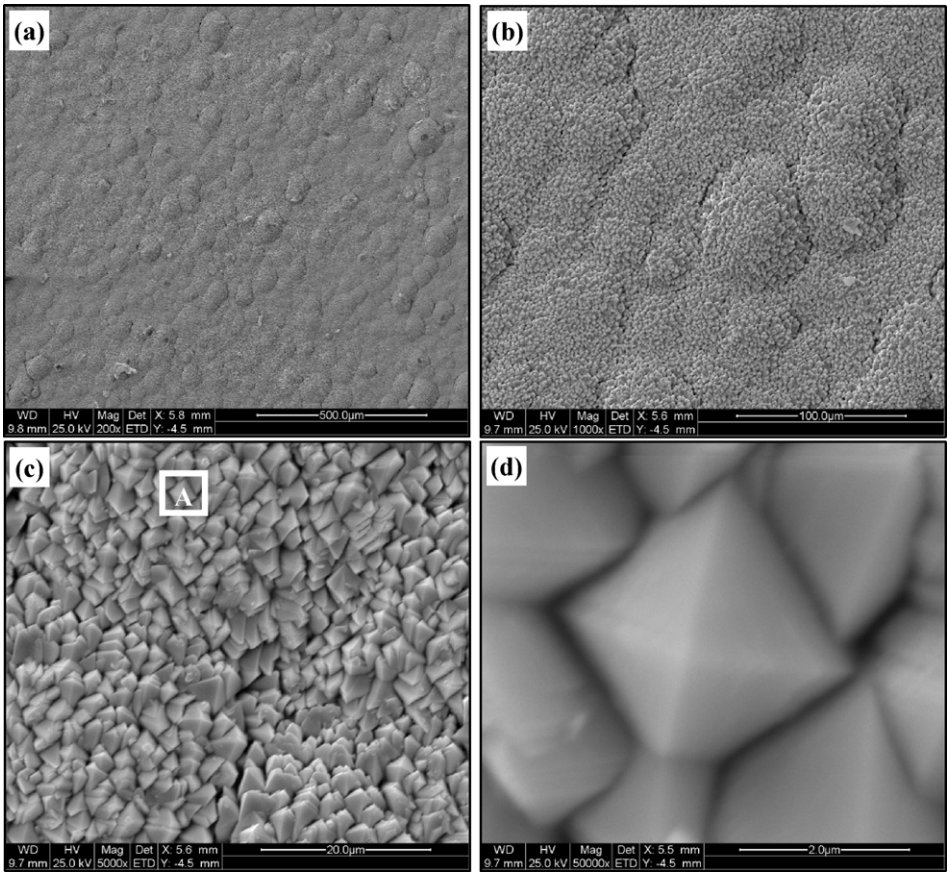

Fig. 3. SEM micrographs of the as-deposited DCL coating top surface with different magnifications: (a) 200×, (b) 1000×, (c) 50,000× and (d) 5,00,000×, the selected location A of (c).

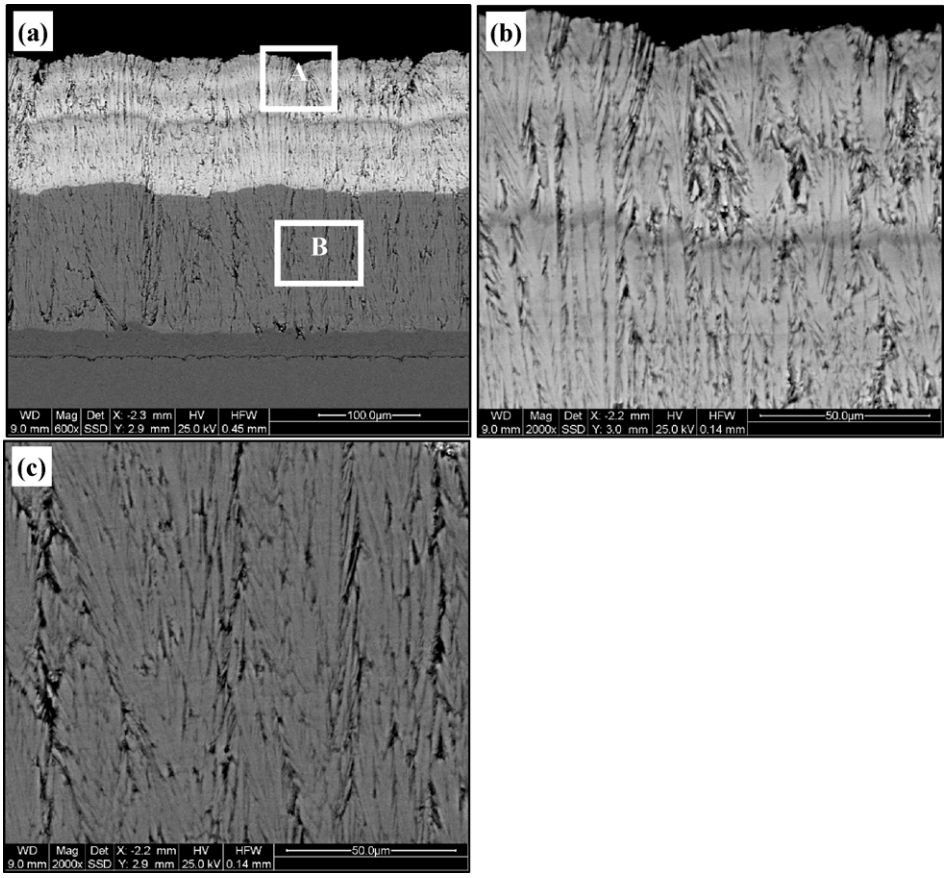

Fig. 4. (a) The fractured cross section SEM micrograph of the as-deposited DCL coating. (b and c) The enlarged images of areas A and B in (a).

3.2. Microstructure of DCL coating

Fig. 3 shows the top surface SEM images of the as-deposited DCL coating. The column tips exhibit a cauliflower-like appearance as shown in Fig. 3a and b, which is similar to the microstructure reported in Ref. [22]. The surface morphology is basically similar to that of the YSZ coating, which is previously reported in Ref. [23]. Obviously, the gaps introduced due to the "shadowing effect" between column tips are also observed in Fig. 3, which may partially release the concentration of thermal stress during long-term service. Namely, the tip edge of a columnar grain blocks the vapor flux and produces a shadow during rotation, which results in formation of inter-columnar gaps [23]. The clearance of inter-columnar gaps is determined to be about from 0.05 μm to 0.25 μm. The morphology of the column tips has a rather pyramidal shape as shown in Fig. 6c and d, which refers to the cubic lattice of the pyrochlore and/or fluorite compound. The pyramids are oriented in plane so that their diagonal edges, corresponding to the intersection of <0 0 1> planes with the surface, are either parallel or perpendicular to the rotation axis. The pyramidal diameters are measured to be approximately 1.5–3.5 μm, which is smaller than that of single LZ7C3 coating as observed in our previous investigation [10]. The possible reason is that the nucleation growth of randomly oriented LZ7C3 grains within single and DCL system begins with different substrate materials. The substrate temperature for the YSZ bottom layer during deposition is relatively higher than that of bond coat. The higher is the substrate temperature, the faster is the surface diffusion of the atoms. On the other hand, the difference of the substrate temperature probably has important effects on the solidification, nucleation and growth of grains.

It can be seen from Fig. 4 that the feather-like microstructure within the columns normal to the bond coat surface is a representative morphology of the coating made by EB-PVD, and such a columnar structure has a very high tolerance to thermal cycling and is further helpful in improvement of thermal cycling life [24]. It is also found that each column consists of a number of subcolumns with different misorientations and each column is irregularly distributed and length of each feather-arm is different from each other (Fig. 4b and c). Differences in vapor pressure of the constituents could result in formation of bubbles into the melting pool and then lead to spitting of liquid droplets from the melting pool onto the substrate. This results in inhomogeniety in the coating microstructure [24]. The inter-columnar gaps with a width of 0.85–1.15 μm are existed in both of two layers. However, it can be seen from Fig. 4b and c that a bit of bridging of the columns within DCL coating can lead to a reduction in strain tolerance and hence may affect TBCs life. In addition, a branched columnar structure is clearly observed in Fig. 4a. The columns of LZ7C3 coating are more irregularly distributed and the intercolumnar gaps are larger than those of the YSZ coating. There is no doubt that such a disordered structure of LZ7C3 coating is beneficial to the reduction of thermal conductivity and hence improves the thermal insulation of TBCs. It can be carefully observed from Fig. 4b and c that the columnar morphologies between two layers seem to be different. This phenomenon could be related to the averaged substrate temperature adopted during deposition in combination with the relation of $0.3\,T_m < T_s < 0.5\,T_m$ (T_s: substrate temperature, T_m: melting point) [25]. In addition, the morphology of vapor deposited coatings is generally controlled by multiple processing variables including: adatom kinetic energy, adatom angle of incidence, deposition rate, the presence and nature

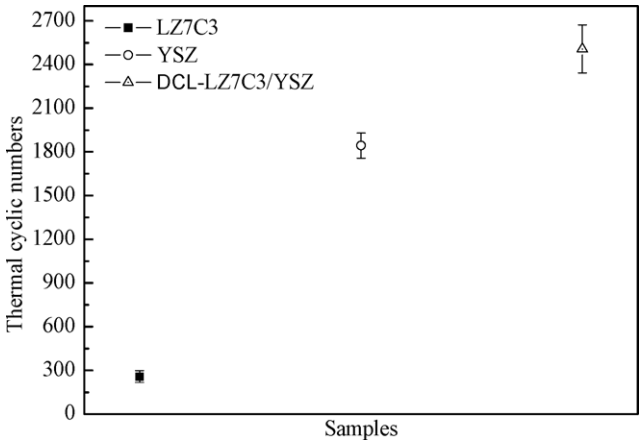

Fig. 5. Comparison of thermal cycling lives of LZ7C3, YSZ and DCL-LZ7C3/YSZ coatings.

of the surrounding gas, elemental compositions of the adatoms, substrate roughness and the relative amount of chamber ionization generation [19,26].

3.3. Thermal cycling behavior of DCL coating

In order to evaluate the performance of DCL coating, the thermal cycling tests of single LZ7C3 and single YSZ coatings were also conducted under the same conditions. The thermal cycling life of each coating is the averaged value of three samples. Thermal cycling lives of LZ7C3, YSZ and DCL coatings are compared in Fig. 5. The DCL coating has an average lifetime of 2507 cycles which corresponds to a total cycling time of ~293 h, exhibiting a significant improvement in the thermal cycling life. Its thermal cycling life is not only much longer than that of LZ7C3 coating, but also approximately 27% longer than that of YSZ coating. The long lifetime of the DCL coating could be mainly attributed to the effective reduction of the thermal expansion mismatch between bond coat and LZ7C3 coating, and the sintering-resistance of LZ7C3 top layer can also provide good thermal protection for the YSZ bottom layer [9]. Additionally, thermal stresses generated in the DCL coating are probably lower than that in the single YSZ TBCs. Therefore, it can be expected that the resistance to thermal cycling of the DCL TBCs can be significantly improved. The premature failure of single LZ7C3 coating can be mainly related to the chemical incompatibility of LZ7C3 coating and TGO layer and its sharp decrease of thermal expansion coefficient at low temperature ($6.59 \times 10^{-6}\,K^{-1}$, 538 K) [10,11]. The failure behaviors of single LZ7C3 coating in this study are similar to our previous investigation at 1373 K in an air furnace [16].

During thermal cycling, failure occurred by a large area of coating as illustrated in Fig. 6, accounting for much more than 5% of the specimen area, peeling off in one piece instead of the coating spalling bit by bit, and this occurred within the last tens of cycles. The large surface macro-cracks could be clearly observed in DCL coating after failure as shown in Fig. 6b. Meanwhile, the "white zone" appeared in Fig. 6b is possible to the occurrence of the YSZ bottom layer. Additionally, the re-crystallization of some LZ7C3 fine grains is also observed at several locations. The re-crystallization would make volume contraction for LZ7C3 coating, and this may lead to the macro-cracks formation in the early stage of thermal cycling. With the thermal cycling going on, the stresses due to CTE difference and temperature gradient accompanied the lower fracture toughness values would result in the pre-existing cracks development in the LZ7C3 coating. It can be seen from the edge chipping of the ceramic coating (Fig. 6b) that all the DCL coatings seem to have the same failure mode, probably occurring at the interface between the ceramic top coat and bond coat.

Fig. 7 shows the SEM images of the DCL coating surface after failure and corresponding EDS analyses. Although grain boundaries between columnar grains have disappeared to a certain extent after ~2507 cycles, column tips still present cauliflower-like appearance that is the characteristic microstructure of EB-PVD coating, indicating that LZ7C3 material has a good thermal cycling behavior and low sintering ability. This phenomenon is consistent with the results reported in Ref. [8]. It means that the new DCL coating with the LZ7C3 layer on top of the YSZ layer exhibits good thermal protection. It is worth emphasizing that partial densification is also observed in Fig. 7a–c, implying that the elemental interdiffusion induced by concentration gradient between the two layers is likely to affect the sintering-resistance of the coatings. The densified coatings can also reduce thermal stress/strain tolerance, which will have significant opposite effect on TBCs durability [27]. As presented in Fig. 7a–c, the microcracks with a width of about 5.21–19.71 μm originated on the surface of the top ceramic coating are much more than those of the as-deposited one (Fig. 3a). Mostly, the microcracks are not observed for the latter one. The possible reason is that the top ceramic coating is subjected to a tensile stress during heating. Microcracks between columnar grains could

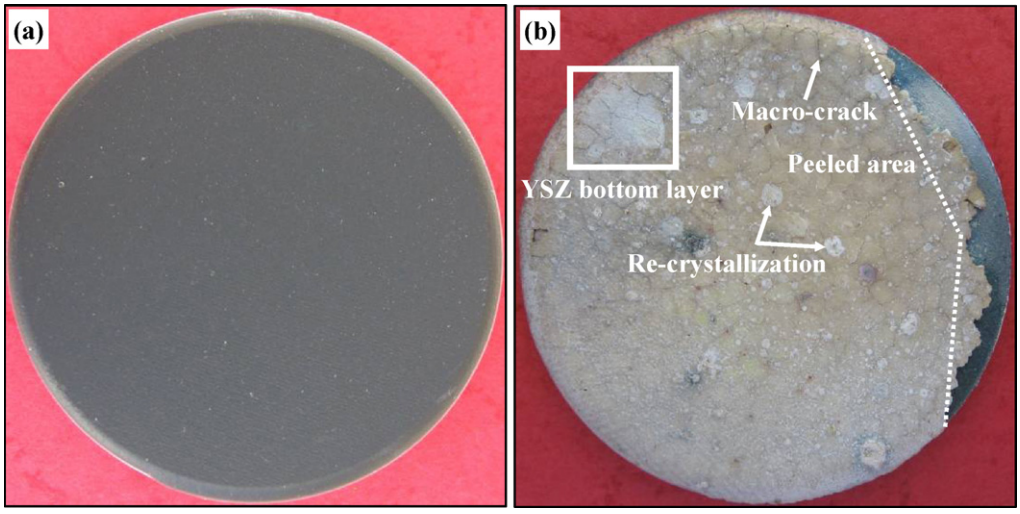

Fig. 6. Surface macro-photos of DCL coatings (a) before and (b) after thermal cycling failure, the white line is shown as the boundary for the peeled area.

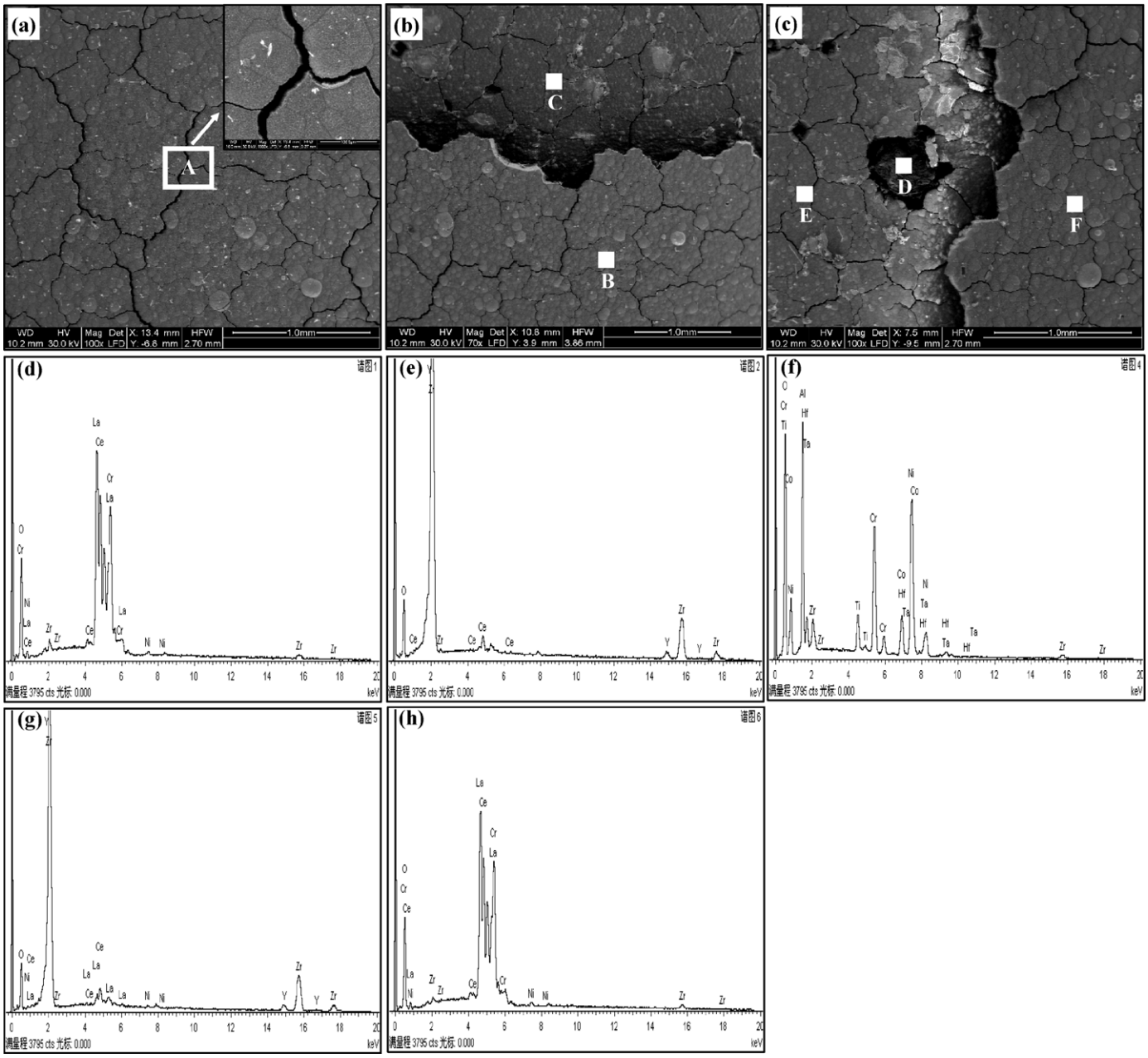

Fig. 7. (a–c) SEM surface morphologies of the DCL coating after spallation failure during thermal cycling test. (d–h) EDS spectra of areas "B" to "F", respectively. Inset of panel (a) is the enlarged image of area A.

be easily induced because microcracks are able to release stresses in the ceramic coating [28]. It is expected that those micro-cracks would be beneficial in extending the thermal cycling lifetime of TBCs when they do not grow on a large-scale [29]. In addition, one explanation for the occurrence of microcracks could be attributed to the reduction–oxidation of cerium oxide. By combination of XRD result described in Fig. 1b, it can be deduced that chemical reaction of $2Ce_2O_3 + O_2 = CeO_2$ would occur in the DCL coating during thermal cycling. The LZ7C3 ingot is heated in vacuum by electron beam source during deposition, which is a reduced atmosphere and the cerium oxide is reduced to Ce^{3+} to a certain extent. When the reduced cerium oxide is annealed in air, it would be oxidized again and the coating would swell. Therefore, the microcracks are easy to be formed due to the presence of cerium in both Ce^{3+} and Ce^{4+} oxidation states within the coating surface.

Furthermore, several micro-cracks are carefully observed inside of the coatings as shown in Fig. 7b and c, and the coatings' surface is simultaneously divided into several layers, implying that the spallation of DCL coating induced by transverse cracks may be the first emergence of delamination followed by spalling layer by layer. From Fig. 7f, the delamination of the DCL coating is clearly observed after spallation failure. The EDS analysis of area "D" (Fig. 7f) shows that the relative contents of Al, Ni, Cr, Co and O are high, but contents of other elements such as Zr, Hf, Ti and Ta are low, indicating that the spallation location of the DCL coating probably occurs in the interface of YSZ and bond coat (Spallation "D"). In other words, bond coat oxidation is still an important factor for DCL coating failure. On the other hand, the representative EDS results presented in Fig. 7e and g show that the relative contents of Y, Zr and O are very high, only few of elements of Ce and Ni are also detected, implying

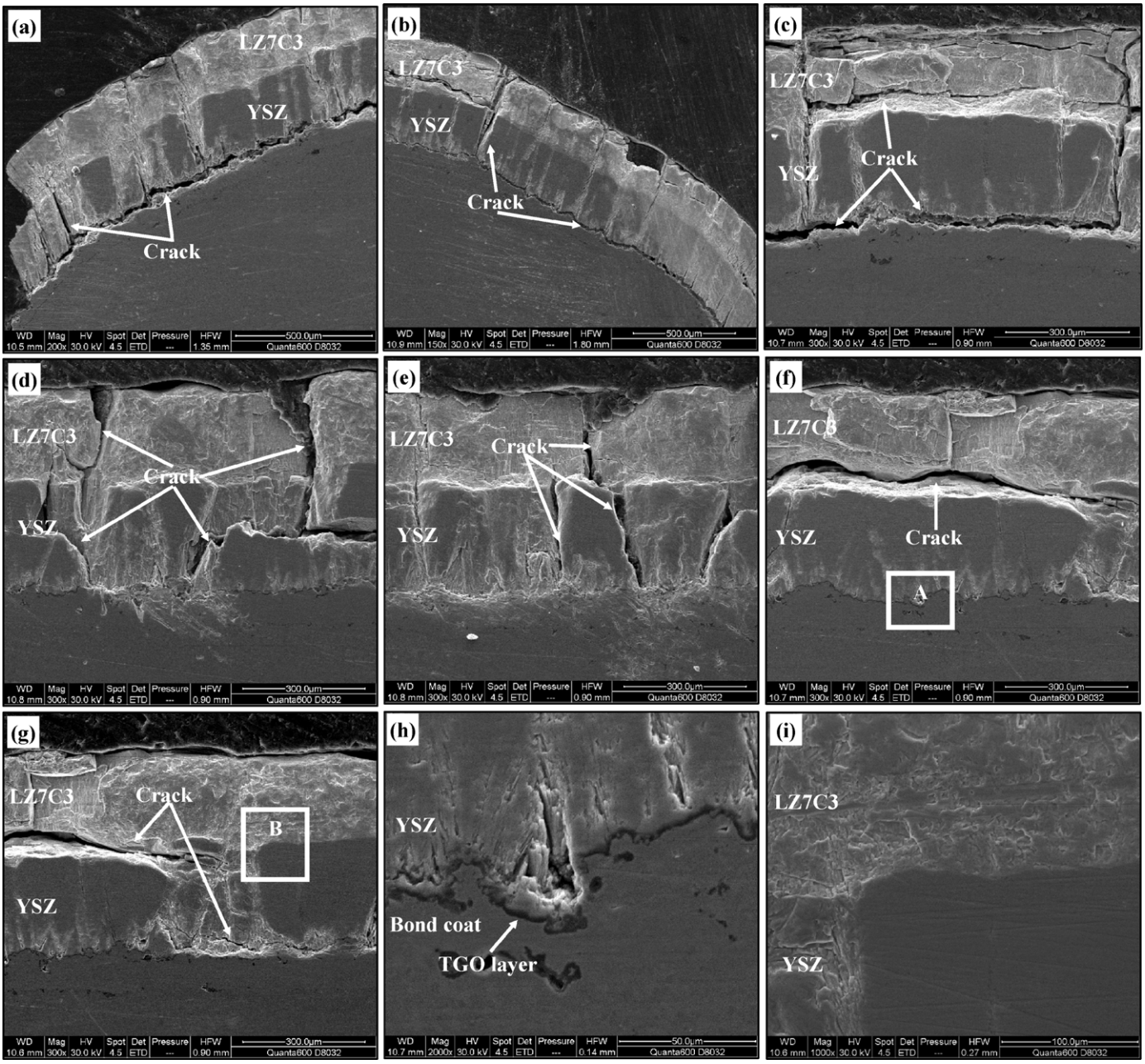

Fig. 8. (a–g) Cross-sectional SEM images of the DCL coating after spallation failure during thermal cycling test. (h) and (i) The enlarged images of areas A and B, respectively.

that YSZ still exists on the surface of the Spallation areas "C" and "E". This phenomenon is in good agreement with the result gained in Figs. 2 and 6b. It demonstrates that the spallation location is likely to occur either at the interface between LZ7C3 and YSZ layers or inside of the YSZ bottom layer. The exposed YSZ layer at temperature above 1573 K could age dramatically including shrinkage and microcrack formation. The degradation could lead to an increase of the Young's modulus of the coating. The increase in Young's modulus during thermal cycling is an indicator for the loss of tolerance against differing thermal expansion coefficients of YSZ layer and bond coat, and then leads to a peeling off of the YSZ layer. Surprisingly, it can be careful seen from Fig. 7d and h that the metallic elements of Ni and Cr appear in the areas "A" and "F", implying that the alloying elements of Ni and Cr in bond coat may have partially diffused out and even extend to the LZ7C3 layer.

The cross-sectional SEM images of the DCL coating after thermal cycling test are presented in Fig. 8. After thermal cycling, a black thin layer with a thickness of ~2.58 μm between the YSZ layer and bond coat is clearly observed in Fig. 8a–h, and this thin layer is so-called as the thermally grown oxide (TGO) layer, implying that bond coat oxidation is still an important factor for coating failure. The thickness of TGO layer observed in this study after failure is much thinner than that of one reported in our previous investigation [16]. The internal-oxidation of bond coat usually occurs by both the oxygen penetration through the inter-columnar gaps in the ceramic coating and oxygen-diffusion through the crystal lattice of the coating material [30]. It seems that this phenomenon is consistent with the results shown in Fig. 7c and f. The TGO layer consists of mainly Al_2O_3 and some oxides of Ni, Cr and Co as proved by EDS, whose data is not shown in this paper. It is generally known that the location of delamination and cracks is mostly within the TGO layer for EB-PVD coatings. Delamination cracks run through the oxide pegs mostly connecting locations that have a thin TGO, and therefore preferentially along the TGO/bond coat interface [31].

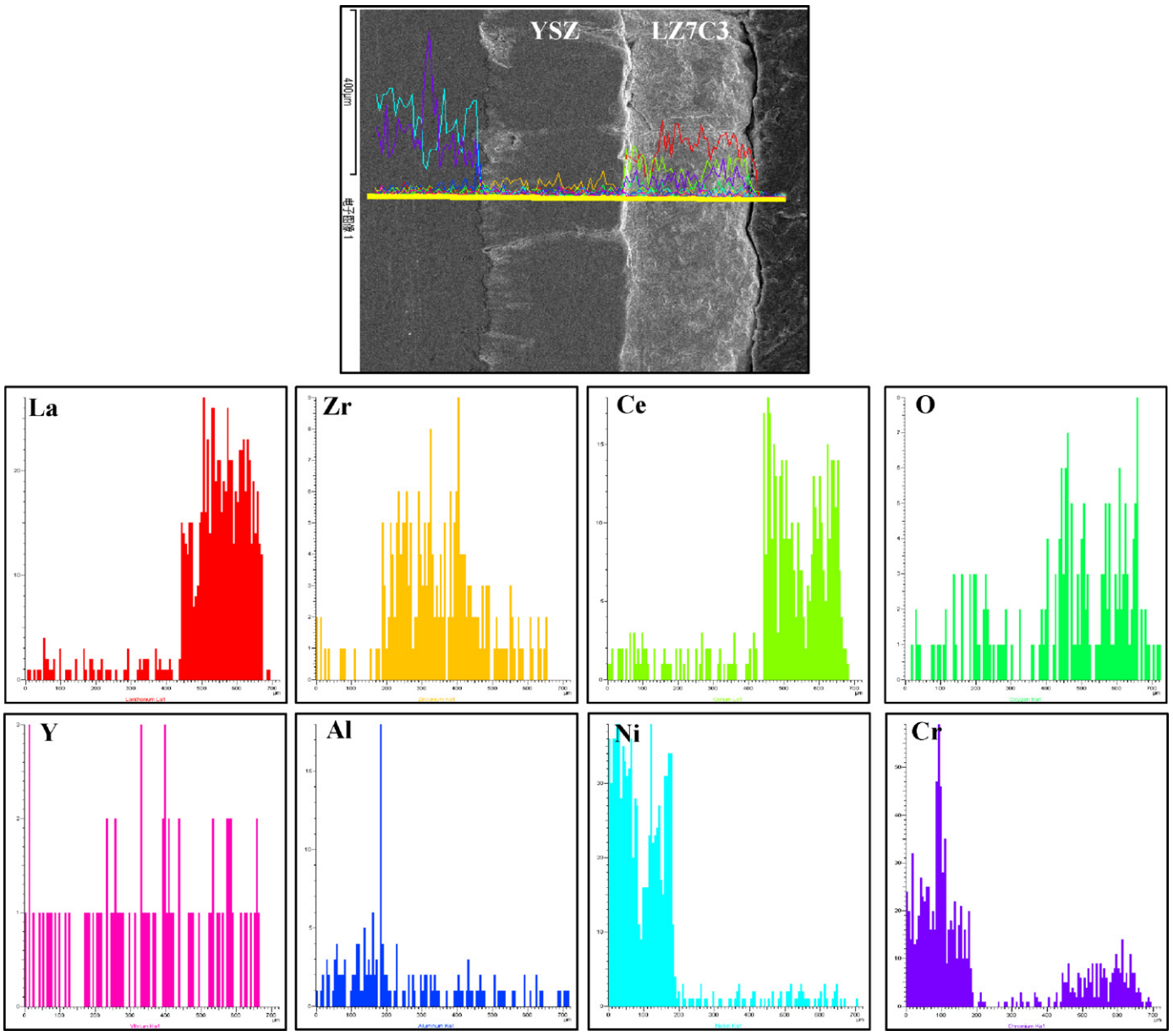

Fig. 9. SEM micrograph of the cross section and the corresponding elemental analysis by EDS for DCL coating which is still perfect without serious spallation after thermal cycling.

With the increment of the cyclic time, cracks further propagate and then result in the distinct separation of interface as observed in Fig. 8h. Moreover, as shown in Fig. 8a–c significant delamination at the TGO/bond coat interface will have a significant impact on the durability of the TBCs, and further lead to TBCs delamination. The additional stress, i.e. growth stress, associated with the TGO growth is one of the main factors for the crack growth and spallation failure of TBCs [32].

The interfacial thermal stress is the main factor of crack initiation and extension. If the stress state exceeds the adhesive or cohesive bond strength of the coating, delamination and spallation may occur [33]. Fig. 8b, c, f and g exhibits a typical cleavage at the interface between the LZ7C3 and YSZ layers, which is probably initiated by the compressive stresses in the cooling process. It is considered that when the compressive stresses are built up so much that become larger than the combination force of the LZ7C3/YSZ coatings' interface during thermal cycling, the spallation will occur by disconnection of the LZ7C3 top layer from the YSZ bottom layer. However, the interface of LZ7C3/YSZ observed in Fig. 8i is intact even after long-term exposure, implying that the disconnection of the interface of LZ7C3/YSZ is not appeared through all the locations for DCL coating. It can be seen from Fig. 8b–g that transverse cracks occur not only at the interface between the LZ7C3 and YSZ layers, but also in the interior of the LZ7C3 and YSZ layers. These phenomena are in accord with the results mentioned in Figs. 6b, 7e and g. Because micro-cracks are able to release stresses introduced into both ceramic layers, however, the growth of the micro-cracks to macro-cracks is expected to cause the failure of the coating. Meanwhile, several transverse cracks and spallation zones inside of LZ7C3 layer appeared in Fig. 8a–e illustrate that the failure of DCL coating may initiate at the surface of LZ7C3 coating due to partial sintering of LZ7C3 coating surface after long-term cycling, which results in parallel contraction of LZ7C3 coating surface. The plane tensile stress is developed in the outer region of LZ7C3 coating due to the restriction of the inner region of its coating upon thermal cycling [34]. The transverse cracks in the outer region of

LC7C3 coating are developed when the plane tensile stress is accumulated to a certain extent, leading to the spallation of the outer region of LZ7C3 coating. This process is repeated and LZ7C3 coating spalls gradually layer by layer. This result effectively explains why the multi-layer structures are formed within the coating surface as shown in Fig. 7b and c. On the other hand, it is also observed in Fig. 8c, d and g that the vertical cracks run through the two layers and further propagate down to bond coat surface. As a consequence, the occurrence of transverse cracks within bond coat surface causes abnormal oxidation of bond coat and builds up stress growth due to volume swelling, which could reduce the adhesion strength of the interface between the YSZ bottom layer and bond coat. In this case, it is considered that air goes through those cracks to reach bond coat surface, and causes the abnormal oxidation of bond coat [35]. Therefore, a transverse (or vertical) crack develops when the stress, i.e. thermal stress, is accumulated to some extent, leading to the initiative spallation of YSZ layer in DCL system. In addition, the match in coefficient of thermal expansion either between LZ7C3 and YSZ layers or YSZ and TGO layers is regarded as one of primary factors to influence on the thermal cycling life of DCL coating [15]. Hence, it is reasonable to suppose that a larger thermal expansion mismatch contributes to increasing of the residual stress and strain energy release rate for cracking at the interface either between LZ7C3 and YSZ layers or YSZ and TGO layers when TBCs is cooled down from operation temperature to ambient.

The elemental distributions along the cross section of DCL coating and at the YSZ/bond coat interface are analyzed by means of EDS and the results are shown in Fig. 9. As expected, TGO is rich in Al and O. The high contents of Al and O extend to a distance of approximately several micrometers from TGO towards bond coat, implying that bond coat has been deeply oxidized during long-time thermal cycling. As seen from Fig. 9, a bit of Y element has diffused into the LZ7C3 top layer after long-term exposure. It is considering that the Y incorporation into LZ7C3 coating is probably an important lifetime governing factor of TBCs which results in a decrease of the Y content in the YSZ layer. If the Y concentration is reduced beneath a critical level, its positive effect on the stability of t'-phase in YSZ layer is lost, resulting in DCL failure. Surprisingly, the alloying element of Cr in bond coat has partially diffused out and even extends to the LZ7C3 layer as shown in Fig. 9. As previously reported by Thornton [36], partial reduction of the Ce^{4+} ions to Ce^{3+} may be possible by chromium in the bond coat, and the relevant relationship can be expressed as:

$$6CeO_2 + 2Cr = 3Ce_2O_3 + Cr_2O_3 \quad (1)$$

The heating of LZ7C3 layer on a chromium-containing coat is expected to result in the reduction of the Ce^{4+} ions in the LZ7C3 layer to Ce^{3+} ions. Meanwhile, occurrence of microcracks in the LZ7C3 layer due to the reduction–oxidation of cerium oxide and a corresponding number of oxygen vacancies in the lattice are also induced. Thus there is a large area capable of taking oxygen from the LZ7C3 layer. This phenomenon is in good agreement with the result mentioned in Fig. 7d and h. On the other hand, the existence of Cr_2O_3 can also lead to the formation of $LaCrO_3$. As previously reported by Hashimoto [37], the crystal structure of $LaCrO_3$ below 513 K and above 553 K is orthorhombic- and rhombohedral-distorted perovskite structure, respectively. The discrete volume compression is observed at the phase transition from orthorhombic to rhombohedral phase, which might generate internal stresses and initiate microcracks within the ceramic coatings during heating-up and cooling-down. Similarly, the alloying element of Ni in bond coat has partially diffused out and even extends to the LZ7C3 layer (Fig. 9). This phenomenon is consistent with the results as obtained in Fig. 7d, g and h. The outward diffusion of Ni element can be easy to the formation of $LaNiO_3$ within the LZ7C3 top layer. $LaNiO_3$ has a single perovskite structure below 1273 K. At temperatures of above 1273 K, the following sequence of decomposition occurs upon increasing temperature: $LaNiO_3 \rightarrow La_4Ni_3O_{10} \rightarrow La_3Ni_2O_7 \rightarrow La_2NiO_4$ as confirmed previously by Zinkevich [38]. This process could be detrimental to the ceramic coating, because the temperature adopted for thermal cycling is 1573 K. Therefore, the outward diffusion of alloying element may eventually lead to premature failure of DCL coating.

4. Conclusions

Novel TBCs based on DCL coating of LZ7C3/YSZ were deposited by EB-PVD and the thermal cycling behavior was systematically investigated. The conclusions we achieved are as follows:

(1) The DCL coating has an average lifetime of 2507 cycles when exposes to gas flame, equaling to a holding time of ~293 h, exhibiting a significant improvement in the thermal cycling life. The DCL coating has a longer thermal cycling life than that of the single layer coating of LZ7C3 or YSZ, indicating a promising potential as new TBC materials.
(2) The low sintering ability of LZ7C3 coating and the unique growth modes of columns within DCL coating, which are all very helpful to the prolongation of thermal cycling life of DCL coating.
(3) The reduction–oxidation of cerium oxide (Ce_2O_3 and CeO_2), the re-crystallization of some LZ7C3 fine grains, the visible cracks initiation, propagation and extension, the abnormal oxidation of bond coat, the degradation of t'-phase in YSZ layer and the outward diffusion of alloying element into LZ7C3 layer are the primary factors for the spallation of DCL coating.

Acknowledgements

The authors gratefully acknowledge the careful manufacture of bond coats by X.Y. Shang. Financial supports from projects NSFC-50825204 and NSFC-20921002 are also gratefully acknowledged.

References

[1] Z.-G. Liu, J.-H. Ouyang, Y. Zhou, X.L. Xia, J. Eur. Ceram. Soc. 29 (2009) 2423–2427.
[2] H.B. Zhao, M.R. Begley, A. Heuer, R. Sharghi-Moshtaghin, H.N.G. Wadley, Surf. Coat. Technol. 205 (2011) 4355–4365.
[3] Z.-G. Liu, J.-H. Ouyang, Y. Zhou, Mater. Lett. 62 (2008) 3524–3526.
[4] Z.H. Xu, L.M. He, R.D. Mu, S.M. He, G.H. Huang, X.Q. Cao, Surf. Coat. Technol. 204 (2010) 3652–3661.
[5] Z.-G. Liu, J.-H. Ouyang, Y. Zhou, S. Li, J. Eur. Ceram. Soc. 30 (2010) 2707–2713.
[6] X.Q. Cao, R. Vassen, F. Tietz, D. Stöver, Adv. Mater. 15 (2003) 1438–1442.
[7] H. Dai, X.H. Zhong, J.Y. Li, J. Meng, X.Q. Cao, Surf. Coat. Technol. 201 (2006) 2527–2533.
[8] S. Sodeoka, M. Suzuki, T. Inoue, K. Ueno, S. Oki, Proceedings of the 9th National Thermal Spray Conference on Practical Solutions for Engineering Problems, 1996, pp. 295–302.
[9] X.Q. Cao, J.Y. Li, X.H. Zhong, J.F. Zhang, Y.F. Zhang, R. Vassen, D. Stöver, Mater. Lett. 62 (2008) 2667–2669.
[10] Z.H. Xu, L.M. He, R.D. Mu, S.M. He, X.H. Zhong, X.Q. Cao, J. Eur. Ceram. Soc. 29 (2009) 1771–1779.
[11] Z.H. Xu, L.M. He, X.H. Zhong, R.D. Mu, S.M. He, X.Q. Cao, J. Alloys Compd. 478 (2009) 168–172.
[12] S. Lakiza, O. Fabrichnaya, C. Wang, M. Zinkevich, F. Aldinger, J. Eur. Ceram. Soc. 26 (2006) 233–239.
[13] Z.-G. Liu, J.-H. Ouyang, Y. Zhou, J. Li, J. Alloys Compd. 468 (2009) 350–355.
[14] R. Vassen, M. Dietrich, H. Lehmann, X. Cao, G. Pracht, F. Tietz, Mater. Sci. Eng. Technol. 32 (2001) 673–677.
[15] H. Dai, X.H. Zhong, J.Y. Li, Y.F. Zhang, J. Meng, X.Q. Cao, Mater. Sci. Eng. A 43 (2006) 1–7.
[16] Z.H. Xu, S.M. He, L.M. He, R.D. Mu, G.H. Huang, X.Q. Cao, J. Alloys Compd. 509 (2011) 4273–4283.
[17] B. Saruhan, P. Francois, K. Fritscher, U. Schulz, Surf. Coat. Technol. 182 (2004) 175–183.
[18] W. Ma, S.K. Gong, H.B. Xu, X.Q. Cao, Surf. Coat. Technol. 200 (2006) 5113–5118.
[19] U. Schulz, B. Saruhan, K. Fritscher, C. Leyens, Int. J. Ceram. Technol. 1 (4) (2004) 302–315.

[20] B.P. Manda, V. Grover, M. Roy, A.K. Tyagi, J. Am. Ceram. Soc. 90 (2007) 2961–2965.
[21] V. Lughi, D.R. Clarke, J. Am. Ceram. Soc. 88 (2005) 2552–2558.
[22] K. Bobzin, E. Lugscheider, N. Bagcivan, High Temp. Mater. Process. 10 (2006) 103–108.
[23] U. Schulz, S.G. Terry, C.G. Levi, Mater. Sci. Eng. A 360 (2003) 319–329.
[24] R. Subramanian, S.M. Sabol, J. Goedjen, M. Arana, ATS Review Meeting, November 8–10, 1999.
[25] B.A. Movchan, A.V. Demischin, Phys. Met. Metallogr. 28 (1968) 83–90.
[26] U. Leushake, T. Krell, U. Schulz, M. Peters, W.A. Kaysser, B.H. Rabin, Surf. Coat. Technol. 94–95 (1997) 131–136.
[27] N.P. Bansal, D.M. Zhu, Surf. Coat. Technol. 202 (2008) 2698–2703.
[28] R.J.L. Steenbakker, R.G. Wellman, J.R. Nicholls, Surf. Coat. Technol. 201 (2006) 2140–2146.
[29] X. Bi, H. Xu, S. Gong, Surf. Coat. Technol. 130 (2000) 122–127.
[30] R.A. Miller, Surf. Coat. Technol. 30 (1987) 1–11.
[31] U. Schulz, M. Menzebach, C. Leyens, Y.Q. Yang, Surf. Coat. Technol. 146–147 (2001) 117–123.
[32] R. Vassen, G. Kerkhoff, D. Stöver, Mater. Sci. Eng. A 303 (2001) 100–109.
[33] J.W. Hutchinson, A.G. Evans, Surf. Coat. Technol. 149 (2002) 179–184.
[34] W. Ma, S.K. Gong, H.F. Li, H.B. Xu, Surf. Coat. Technol. 202 (2008) 2704–2708.
[35] H. Xu, S. Gong, L. Deng, Thin Solid Films 334 (1998) 98–102.
[36] J. Thornton, A. Majumdar, G. McAdam, Surf. Coat. Technol. 94–95 (1997) 112–117.
[37] T. Hashimoto, N. Tsuzuki, A. Kishi, K. Takagi, K. Tsuda, M. Tanaka, K. Oikawa, T. Kamiyama, K. Yoshida, H. Tagawa, M. Dokiya, Solid State Ionics 132 (2000) 183–190.
[38] M. Zinkevich, N. Solak, H. Nitsche, M. Ahrens, F. Aldinger, J. Alloys Compd. 438 (2007) 92–99.